Mechanical transformation of fullerene (C60) to aqueous nano-C60 (aqu-nC60) in the presence and absence of light

ARTICLE *in* JOURNAL OF NANOPARTICLE RESEARCH · OCTOBER 2013

Impact Factor: 2.18 · DOI: 10.1007/s11051-013-2069-4

4 AUTHORS:

Paul Indeglia
Agency for Sustainable Systems in Scie…
8 PUBLICATIONS **39** CITATIONS
SEE PROFILE

Vijay Krishna
Cleveland Clinic
34 PUBLICATIONS **591** CITATIONS
SEE PROFILE

Angelina Tsenova Georgieva
Orlando Socrates Preparatory School
35 PUBLICATIONS **334** CITATIONS
SEE PROFILE

Jean-Claude J Bonzongo
University of Florida
74 PUBLICATIONS **1,787** CITATIONS
SEE PROFILE

J Nanopart Res (2013) 15:2069
DOI 10.1007/s11051-013-2069-4

RESEARCH PAPER

Mechanical transformation of fullerene (C_{60}) to aqueous nano-C_{60} (*aqu-n*C_{60}) in the presence and absence of light

Paul A. Indeglia · Vijay B. Krishna · Angelina Georgieva · Jean-Claude J. Bonzongo

Received: 22 July 2013 / Accepted: 11 October 2013 / Published online: 25 October 2013

Abstract The present study was carried out to evaluate transformation kinetics of derivatized fullerene species by simulating natural aquatic processes, which will help elucidate biological effects of water-stirred nano-C_{60} (*aqu-n*C_{60}). Physicochemical analyses of *aqu-n*C_{60} included molecular and agglomerate-scale characterization, surface charge analysis through examination of electrophoretic mobility, and chemical composition analysis using spectroscopy. Detailed analysis of *aqu-n*C_{60} transformation over a 28-day stirring period in both light and dark conditions indicated *aqu-n*C_{60} agglomerate concentrations can be estimated as a time-function using a predictor model ($R^2 > 0.99$). Number-weighted agglomerate size did not differ significantly over the 28-day stirring period regardless of photocondition, although size distributions were more uniform as stirring time increased. The total number of surface groups identified through XPS indicated increased derivatization as a function of time with additions assigned to mono-oxygenated carbon moieties while the number of di-oxygenated moieties declined. Earlier-phase stirring ($t \leq 14$ days) products were shown to contain epoxide surface groups, which were absent in later-phase ($t > 14$ days) suspensions, suggesting specific pathways to derivatization with preferential mono-oxygenated states. Filter residue, a by-product of the *aqu-n*C_{60} synthesis process, demonstrated high hydrophobicity and FTIR spectra similar to underivatized material, suggesting synthesis process inefficiencies.

Keywords Nanoparticles · Fullerene · Characterization · Spectrometry · Derivatization · By-products · Colloids · Toxicological effects

Electronic supplementary material The online version of this article (doi:10.1007/s11051-013-2069-4) contains supplementary material, which is available to authorized users.

P. A. Indeglia (✉) · J.-C. J. Bonzongo
Department of Environmental Engineering Sciences, University of Florida, Gainesville, FL, USA
e-mail: indeglia@gmail.com

Present Address:
P. A. Indeglia
Agency for Sustainable Systems in Science and Technology, Nashua, NH, USA

V. B. Krishna · A. Georgieva
Particle Engineering Research Center, University of Florida, Gainesville, FL, USA

Present Address:
V. B. Krishna
Cleveland Clinic Lerner Research Institute, Cleveland, OH, USA

Introduction

Fullerene (C_{60}) has been researched extensively for applications to exploit its unique structural, electrical, and thermal characteristics (Prylutska et al. 2011; Nardes et al. 2012; Makarova et al. 2012). Fullerene

production has dramatically increased in recent years with current production over a ton annually (Murayama et al. 2004). Underivatized fullerene is insoluble in water (Heymann 1996), which has led to the development of numerous methodologies to increase fullerene dispersability through derivatization of the surface. Underivatized C_{60} has been shown to disperse in turbulent water over a period of days to weeks to form aqueous nano-C_{60} (*aqu*-*n*C_{60}), which has been presented as consisting of only nano-scale agglomerates of C_{60} with a hydrated layer (Deguchi et al. 2001; Andrievsky et al. 2002). In addition to creating a more environmentally transportable product, fullerene derivatization generates waste by-products, which are currently unregulated and can be discharged to the environment. Some researchers have indicated potential adverse toxicological impacts from *n*C_{60} (Oberdorster 2006; Lyon et al. 2006; Zhu et al. 2009), multiple reports have shown enhanced biological effects initiated by fullerene species (Gao et al. 2011; Dai et al. 2012; Baati et al. 2012), and others have indicated that previously reported mechanisms of toxicity required reconsideration (Lyon et al. 2008; Henry et al. 2011), all of which, when viewed comprehensively, suggest the need for additional investigation into toxicological and, a priori, physicochemical characterization. Due to low efficiency in the transformation from raw fullerene to *n*C_{60}, no practical applications have been identified for *n*C_{60} and the material remains primarily as a surrogate for underivatized fullerene in bio-assessment.

Materials under toxicological investigation require extensive physicochemical scrutiny to ascertain size, surface characteristics, chemical composition, and formation dynamics in effort to assess the potential for specific biological responses (Bucher et al. 2004). For example, previous studies have indicated that toxicity of *n*C_{60} transformed with tetrahydrofuran (THF) may be due to residual THF degradation products retained within agglomerates (Henry et al. 2007; Kovochich et al. 2009), obscuring the true biological effects of these materials and elucidating the need for more extensive physicochemical characterization. Research has reported C_{60} to be biologically photo-reactive (Lee et al. 2007; Snow et al. 2012), inviting investigation into the potential for light to impact the type and number of surface groups on the carbon cage, disturbing the non-polar character of underivatized material, and enabling dispersability. Several research groups have used *aqu*-*n*C_{60} in toxicological investigations yet, with limited data on size, surface-chemical composition, and charge distribution reported. Questions remain regarding the impact of synthesis parameters such as stirring duration and photocondition on the formation of end products.

This study examined physicochemical characteristics of *aqu*-*n*C_{60} over a 28-day stirring period with and without exposure to light. A 28-day stirring period was selected to incorporate the stirring times indicated in a majority of the literature reviewed for comparative purposes (Brant et al. 2006; Dhawan et al. 2006; Labille et al. 2006; Markovic et al. 2007). It was hypothesized that both stirring duration and the presence of light impacted mean agglomerate size and size distribution, surface character, and chemical composition of *aqu*-*n*C_{60}. Suspensions of *aqu*-*n*C_{60} were sampled throughout the stirring period and analyzed to assess how the transformation of surface groups was affected by varied preparation times and photoconditions.

Experimental section

Chemicals

C_{60} was obtained from Nano-C (Westwood, Massachusetts) as "nano-c-BF" with 99.5 % purity and solvent-free as reported by the manufacturer (validated with MALDI GC–MS and HPLC). Purity was verified using spectra generated through Renishaw inVia Raman (Hoffman Estates, Illinois) and compared with calculated spectral modes (data not shown) using Gaussian 9 (Wallingford, Connecticut). Magnesium perchlorate ($Mg(ClO_4)_2$) and potassium bromide (KBr) were purchased through Fisher Scientific (Waltham, Massachusetts).

aqu-*n*C_{60} preparation

Synthesis of *aqu*-*n*C_{60} was conducted under both dark and light photoconditions at 22 °C in a protocol used previously (Oberdorster et al. 2004). Briefly, 100 mg of C_{60} were added to 500 mL of de-ionized water and stirred in sealed containers continuously using a

magnetic stirring plate at a mixing rate of 550 rpm, which created a vortex of 50 % height of the water column, a parameter maintained through stirring to accommodate for sample removal. Light-stirred suspensions were maintained for 28 days under ambient light, to replicate natural conditions and previous research (Bouchard et al. 2009), and dark-stirred suspensions were covered with aluminum foil. Light and dark suspensions were prepared simultaneously under identical environmental conditions, photocondition notwithstanding. Aliquots were removed for physicochemical characterization under a vacuum hood before and after filtration using Millipore™ (Billerica, Massachusetts) 0.45 μm-nitrocellulose membranes (Supplementary Information, Figure SI-S1).

Concentration determination

Concentrations of *aqu-n*C_{60} suspensions taken at $t_{7\text{-day}}$, $t_{14\text{-day}}$, and $t_{28\text{-day}}$ under both light and dark photoconditions were determined using ultraviolet (UV) spectrophotometry (absorption at $\lambda = 336$ nm) as described by others (Fortner et al. 2005). Briefly, 0.1 M $Mg(ClO_4)_2$ was added to *aqu-n*C_{60} (2:5 with sample) and vortexed for 15 s/min for 30 min followed by the addition of toluene (1:1 with sample) and supplemental vortexing, transferring underivatized C_{60} into the non-polar solvent phase. The extract was analyzed using the Spectronic GENESYS 10 UV spectrophotometer (Thermo Scientific, Billerica, Massachusetts). Concentrations were determined using a calibration curve prepared with known concentrations of C_{60} in toluene.

Physicochemical characterization

Dynamic light scattering (DLS) using a NanoTrac Particle Size Analyzer (MicroTrac, Inc., York, Pennsylvania) was employed to assess mean agglomerate size (number-weighted) and size distributions using a refractive index of 1.93 (Ruoff et al. 1993; Makarova 2001). Micrographs of *aqu-n*C_{60} agglomerates were obtained through transmission electron microscopy (TEM) using an aluminum standard and a JEOL TEM 200CX (Tokyo, Japan) at 75 kV as a comparative method to assess agglomerate size. The software package, Image J, from the National Institutes of Health (Bethesda, Maryland) was used to count and measure agglomerates within TEM-generated images.

Covered aliquots of stirred suspensions were analyzed three times and in triplicate each day for pH using an Accumet© Research (Pittsburgh, Pennsylvania) AR-50 pH probe, allowing no less than 5 min for stabilization and atmospheric equilibrium to occur to address issues of low ionic content and carbon dioxide adsorption. Zeta potential measurements of *aqu-n*C_{60} suspensions were measured before and after filtration using the Brookhaven ZetaPlus Zeta Potential and Particle Size Analyzer (Holtsville, New York).

Chemical composition of *aqu-n*C_{60} was assessed using ultraviolet/visible light (UV/Vis) spectroscopy, Fourier-transform infrared (FTIR) spectroscopy, and X-ray photoelectron spectroscopy (XPS). Perkin Elmer (Waltham, Massachusetts) UV/Vis Spectrophotometer Lambda 800 was utilized to provide absorption spectra for screening fullerene materials. Thermo (Waltham, Massachusetts) Electron Magna 760 FTIR/FT-Raman/FTIR Microscope was used to generate FTIR spectra within pelletized potassium-bromide to identify surface group types (Kamaras, et al. 1993; Bethune et al. 1999; Hwang and Li 2010; Badireddy et al. 2012). X-ray photoelectron spectroscopic Perkin Elmer PHI 5100 ESCA (Electron Spectroscopy for Chemical Analysis) with an aluminum anode generated binding-energy spectra were used to identify the proportion of surface moieties associated with the fullerene cage. Deconvolution of binding energies from the carbon 1s level (C 1s) spectra was accomplished with AugerScan version 3.2 (RBD Instruments, Inc., Bend, Oregon) to prepare normalized data and Grams/AI version 7.01 (Adept Scientific, Inc., Bethesda, Maryland) for curve-fitting (17-point Sav-Golay smoothing with "high" sensitivity, an "offset" baseline, and the "Mixed Gaussian and Lorentzian" distribution). Binding energies were compared to archived data from the National Institute of Standards and Technology XPS Database (Gaithersburg, Maryland) for identification. Data were analyzed for outliers using Dixon's Q test (Dean and Dixon 1951), normality of data was verified by the Ryan-Joiner normality test, and homogeneity of variance was examined using Bartlett's test. Comparisons of means were conducted using Dunnett's test ($\alpha < 0.05$).

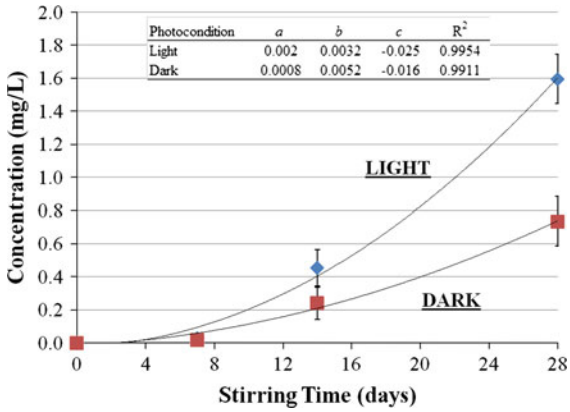

Fig. 1 *aqu-n*C_{60} formation under light and dark photoconditions

Results and discussion

Physicochemical characterization

Estimated concentrations for *aqu-n*C_{60} were 0.016 ± 0.005 mg/L for 7-day dark-stirred (7D), 0.027 ± 0.005 mg/L for 7-day light-stirred (7L), 0.241 ± 0.091 mg/L for 14-day dark-stirred (14D), 0.455 ± 0.104 mg/L for 14-day light-stirred (14L), 0.734 ± 0.138 mg/L for 28-day dark-stirred (28D), and 1.596 ± 0.139 mg/L for 28-day light-stirred (28L). Data were fit to a mathematical relationship in the quadratic form $[m] = at^2 + bt + c$, where $[m]$ is the concentration of *aqu-n*C_{60} (mg/L), t is stirring time, and a, b, and c are coefficients (Fig. 1) with $R^2_{dark} = 0.9911$ and $R^2_{light} = 0.9954$. Mass balance analyses determined 92.7 ± 7.7 % of the initial mass was recovered after dispersion, filter residue, and recovery from the beaker surface ($n = 36$), similar to previous research (Fortner et al. 2005). The remaining fraction was presumed to have been removed from the system via equipment used to dislodge accumulated fullerene material from the sides of the beaker daily, affixed to the glassware, or from sampling methodology error. Fullerene stirred mechanically in water for 28 days formed *aqu-n*C_{60} clusters at concentrations of 1.60 and 0.73 mg/L in light and dark, respectively; the highest concentration reported for *aqu–n*C_{60} in the literature was 11.7 mg/L (Hancock et al. 2012).

Minimum mean agglomerate size of unfiltered *aqu-n*C_{60} assessed by DLS was observed at t_2 for dark-stirred suspensions ($d\mu = 133.2 \pm 34.4$ nm) and at t_6 for light-stirred suspensions ($d\mu = 137.8 \pm 13.6$ nm), while maximum mean agglomerate size was observed for both

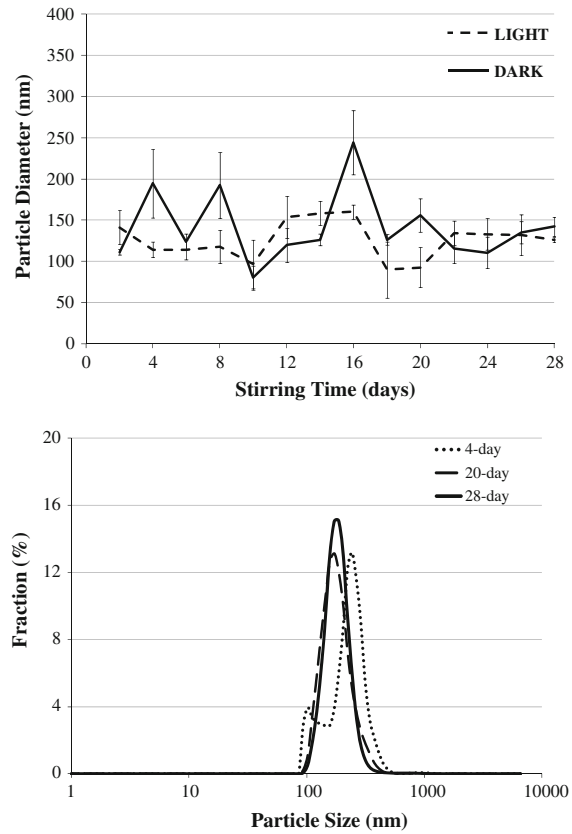

Fig. 2 Size distributions for light-stirred and dark-stirred suspensions over 28 days (*top*) using DLS. Number-weighted agglomerate size distribution for filtered *aqu-n*C_{60} suspensions at t_4, t_{20}, and t_{28} (*bottom*)

suspensions at t_8 of 231.3 ± 142.9 and 224.9 ± 112.5 nm for dark-stirred and light-stirred suspensions, respectively (Fig. 2 and Supplementary Information, Fig. SI-S2 and Table SI-S1). Minimum mean agglomerate size of filtered *aqu-n*C_{60} occurred at t_{10} for dark-stirred suspensions ($d\mu = 80.1 \pm 25.2$ nm) and at t_{18} for light-stirred suspensions ($d\mu = 89.5 \pm 5.4$ nm) with maximum mean agglomerate sizes observed for dark-stirred suspensions of 194.5 ± 71.9 nm (t_4) and for light-stirred suspensions of 160.0 ± 14.5 nm (t_{16}). A generally increasing trend was observed over time although the change from t_2 to t_{28} and the difference between minimum and maximum in either data set were not statistically significant, leading to the conclusion that there was no stirring duration effect on the agglomerate size for unfiltered suspensions. Mean agglomerate size of filtered material were statistically smaller than for unfiltered material, as anticipated from the removal of

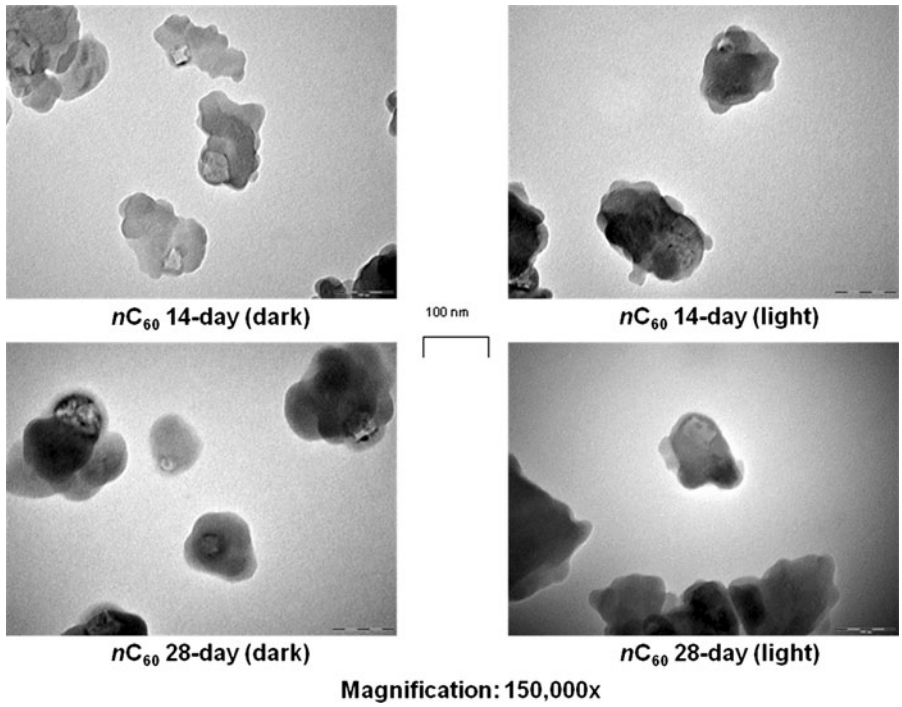

Fig. 3 Transmission electron microscope (TEM) images of *aqu-n*C_{60}. JEOL TEM 200CX (Tokyo, Japan) at 75 kV with an aluminum standard

the majority (>50 %) fraction using a size-exclusion membrane. Agglomerate size distributions indicated a tighter distribution over time with decreasing standard deviations. Mean agglomerate diameters calculated via TEM for filtered *aqu-n*C_{60} were 96.6 ± 10.6, 117.6 ± 9.0, 117.0 ± 12.9, and 108.2 ± 8.8 nm for 14D, 14L, 28D, and 28L suspensions, respectively (Fig. 3), with coefficients of variation in the range of 0.025–0.035, suggesting estimated diameters were in agreement with actual measurements ($\alpha < 0.01$).

Comparison of mean agglomerate size data between DLS and TEM showed consistently the diameter of agglomerates reported by DLS were larger (by 16 % to 35 %) than aggregates measured using TEM. DLS measures hydrodynamic radius which, in most of the cases, is greater than actual particle size since hydrodynamic radii includes the hydrated water layer associated with the particle. Further, electron microscopy requires desiccation of material prior to being introduced to the sample chamber, leading to increased density through the removal of entrained water. Mean aggregate size of similarly prepared *aqu-n*C_{60} determined using DLS images has been reported from 35.1 to 235 nm (Markovic et al. 2007; Tervonen et al. 2010) and using TEM images from 58.6 to 200 nm (Labille et al. 2006; Tervonen et al. 2010), indicating general agreement with previous investigations.

Initial pH measurements at t_0, when underivatized C_{60} was added to de-ionized water, were 5.20 ± 0.70 ($n = 10$). Initially, dark-stirred suspensions experienced a decrease in pH until t_6, when a minimum pH of 4.42 ± 0.59 was reached, after which pH steadily increased to a final ($t_f = 28$ days) value of 6.11 ± 1.08 (Supplementary Information, Figs. SI-S3, SI-S4). The pH of suspensions stirred in light did not decline significantly during the first week but rather stagnated then increased to 6.61 ± 0.87 at t_f. Control samples (de-ionized water only) showed initial pH measurements consistent with treated samples followed by a rapid return to equilibrium by t_8. It should be noted that neither dark-stirred nor light-stirred suspensions achieved the pH of controls over the stirring period, suggesting that these kinetically slow reactions may not have been exhausted at t_f.

The presence of C_{60} slowed the naturally occurring increase of pH, perhaps by binding with available hydroxyl ions, which would have otherwise been consumed to form carbonic acid and, subsequently, carbonate due to its high electron affinity. Mechanic stirring promotes C_{60} aggregate collision, shearing weakly affixed clusters (Ma and Bouchard 2009) and

increasing available hydroxyl binding sites. During a period of approximately 1 week, hydroxylation may have been the dominant force in determining pH of the suspension. However, after approximately 1 week, hydroxylation slowed due to reduced binding sites, indicating carbon dioxide equilibration controlled, but at a markedly slower rate than in the absence of C_{60}.

Increased *aqu-n*C_{60} concentrations in light-stirred suspensions suggested the rate of hydroxylation was greater than in dark-stirred suspensions, which were shown to display a greater reduction in pH during stirring. The opposing forces of hydroxyl consumption through surface hydroxylation and effective hydroxyl generation may have remained equal for the first week of stirring, after which hydroxyl generation may have controlled the rate of pH change until the end of the stirring period. This finding suggests the rate of *aqu-n*C_{60} formation has multiple rate coefficients due to the presence of multiple transformation mechanisms. The generation of reactive oxygen species (ROS) in the presence of derivatized fullerene species with and without irradiation has been described by other researchers (Arbogast et al. 1991; Markovic et al. 2007; Brunet et al. 2009; Kong and Zepp 2012; Qu et al. 2012), generating triplet fullerene ($^3C_{60}$*) and exciting triplet oxygen ($^3O_2$) or singlet oxygen ($^1O_2$) and subsequently the superoxide ion (O_2*–), hydrogen peroxide (H_2O_2–), and hydroxyl species (OH– and OH*). These excitations serve to increase pH, although, as seen through the multiple pathways for formation possible through irradiation, transformation potential was greater when exposed to light. Since it has been proposed that *aqu-n*C_{60} is comprised of underivatized and derivatized fullerene molecules (Fortner et al. 2005) and the concentration of derivatized material was found to increase with time, ROS formation appeared to increase after stirring. The addition of subsequent surface groups to the carbon cage appeared to increase, potentially due to ROS generation, but was tempered through reduced potential binding sites as derivatization proceeded. Generation of radical species not only served potentially to create hydroxyl ions in the presence of C_{60} but may have promoted surface derivatization as well. Future studies of *n*C_{60} solution chemistry may consider use of hydrogen-sensitive glass electrodes and the addition of specialized electrolytes to investigate the role of ionic strength as a function of salt types and concentrations.

Previous researchers reported zeta potential for *aqu-n*C_{60} in the range of −61.8 to −30 mV (Brant et al. 2005, 2006; Dhawan et al. 2006; Bouchard et al. 2009; Chen and Elimelech 2009; Hou et al. 2011; Yang et al. 2012). In this study, zeta potential measurements for unfiltered light-stirred suspensions (Supplementary Information, Fig. SI-S5) ranged from −61.5 to −18.3 mV (−37.8 mV at t_f) and were more electronegative than dark-stirred suspensions with measured values ranging from −49.0 to −17.8 mV (−35.7 mV at t_f). Neither light-stirred nor dark-stirred suspensions changed significantly over time, with standard deviations decreasing during the final week of stirring. Filtered suspensions showed more variability than unfiltered suspensions (Supplementary Information, Fig. SI-S6), characterized by a less neutral charge, and light-stirred suspensions (−48.1 to −18.3 mV) were more negative and stable than dark-stirred suspensions (−42.1 to −4.6 mV). A control of de-ionized water only was established to examine the impact of C_{60} on zeta potential, indicating instability at the beginning of the stirring period (−10.7 mV at t_6), becoming more stable as stirring proceeded (−45.9 mV at t_f). The control likely gained exigent material naturally through infusion of gases, precipitation of residual salts, or atmospheric deposition during sampling and testing; the presence of C_{60} overshadowed these ancillary processes in treated samples.

Filtration increased zeta potential, nominally for light-stirred suspensions but significantly for dark suspensions, suggesting smaller agglomerates were less negatively charged. Based on agglomerate size analysis, which showed tighter distributions over time, it was suggested that smaller agglomerates were more highly derivatized. Therefore, the hydrophilic functional groups on the carbon cage detracted from the overall negative charge of the surface, possibly attributed to functional groups occupying electronegative binding sites. Fullerenes may be more negatively charged initially due to presence of hydroxyl ions in its shear layer, a hypothesis supported by the high electron affinity of fullerene, and through electron transfer reactions; negative charge may migrate through the shear layer to the cage itself. The most probable counterpart at these negative sites would be positive ions; however, the proposed mechanism included electronegative hydroxyl groups, abating this hypothesis. Alternately, the removal of aliquots of

material from the sealed reaction chamber for sampling increased exposure to atmospheric gases; aeration is further enhanced through the filtration process. Dissolved oxygen (DO) levels in de-ionized water recorded during this investigation ($n = 3$) showed oxygen concentrations increased from below 4.0 ± 0.8 mg/L before filtration to near fully saturated at 20 °C after filtration ([DO] $= 8.1 \pm 0.2$ mg/L). High DO increased the partial pressure of O_2, which may have impeded electrophoretic mobility of the agglomerates, or it may have facilitated additional or alternate surface derivatization. Future synthesis activities may seek to investigate the benefits of preparation under controlled atmospheric conditions; however, due to the ultimate goals of determining environmental interactions, exposure to atmospheric conditions are perhaps more relevant.

Chemical composition analysis

Analysis of *aqu-n*C_{60} UV/Vis spectra for suspensions prepared over time and stirred under two photoconditions and before and after filtration was designed to provide useful information on chemical composition during the synthesis process (Supplementary Information, Fig. SI-S7, SI-S8, SI-S9, and SI-S10) as well as on the potential for a cost-effective chemical composition screening methodology. Notable was the presence of two peaks in all suspensions ($n = 168$) at 366 ± 7 and 527 ± 5 nm, corresponding to UV and visible peaks, respectively; these peaks are characteristic of underivatized fullerene (Zhou et al. 1996; Hou and Jafvert 2009a; Lee et al. 2009). Absorption was one magnitude higher in unfiltered suspensions than filtered suspensions, as would be expected from the removal of a significant portion of the material through filtration. Time-series plots of peaks (Supplementary Information, Figs. SI-S11, SI-S12) in the UV range at $\lambda = 360$ nm indicating an increase in intensity at $t \leq 16$ days, after which dark-stirred suspensions declined in absorbance, while light-stirred suspensions continued to increase. The difference between the UV/Vis peak ratios before and after filtration was statistically significant, suggesting filtration removed material in the visible light range that was comprised of more-hydrophobic (less-derivatized) C_{60} was more active in visible light, and the more-hydrophilic (more-derivatized) dispersed material was more active in the UV range.

An analysis of the ratio of absorbances (Supplementary Information, Figs. SI-S13, SI-S14) in UV and visible light peaks (A_{360}/A_{525}), termed the "UV/Vis peak ratio (R_λ)", was conducted to assess the potential to use this parameter as a screening tool for material chemical composition. A similar technique was previously explored for assessing aggregation (Bensasson et al. 1994). The range of UV/Vis peak ratios for the unfiltered material was 0.985–1.036 ($\sigma = 0.012$) for dark-stirred suspensions and 0.999–1.108 ($\sigma = 0.025$) for light-stirred suspensions, while the R_λ for filtered material was 1.359–2.758 ($\sigma = 0.186$) for dark-stirred suspensions and 1.532–2.338 ($\sigma = 0.394$) for light-stirred suspensions. While R_λ for both dark-stirred and light-stirred filtered suspensions trended downward over the stirring period, oscillating variation in the data, more prominent in the dark-stirred suspensions, was possibly a result of analytical error and no statistical significance was determinable. Additional sensitivity analyses were conducted at a variety of wavelength combinations ($R_\lambda = A_{375}/A_{445}$, A_{375}/A_{535}, and A_{445}/A_{535}) with similar results. As seen in the near-unity for the ratio in dark-stirred suspensions over time and the variability in light-stirred suspensions, data did not allow for the establishment of a statistically reliable predictor.

Determination of chemical composition was limited to consideration of non-oxygenated, mono-oxygenated (hydroxyl, epoxide, ether, or ionic oxygen), and di-oxygenated (hemiketal, carbonyl, or carboxylic acid) surface groups (Supplementary Information, Fig. SI-S15). FTIR spectra (Fig. 4 and Supplementary Information, Figs. SI-S16, SI-S17, SI-S18) for all suspensions showed vibrational peaks in distinct ranges (803–880, 940–979, 1001–1006, 1129–1183, 1383–1384, 1428–1460, 1538–1577, 1636–1689, 2364–2368, 2914–2973, and 3172–3627 cm^{-1}), which were assessed in the context of previously published data (Table 1). Spectral peaks in the range of 803–880 cm^{-1} were identified as hydrogenated carbon (C–H), suggesting protonation of the carbon surface or possible sample contamination. Carboxyl groups (Cataldo and Heymann 2006; Fortner et al. 2007), with a peak around 1,740–1,780 cm^{-1}, which may result in structural deterioration of the fullerene, were not identified in any *aqu-n*C_{60} suspension. In addition, carbonyl (Lee et al. 2009; Wang et al. 2012), with a peak around 1,630 cm^{-1}, were absent from the spectra of all suspensions, indicating di-oxygenated groups

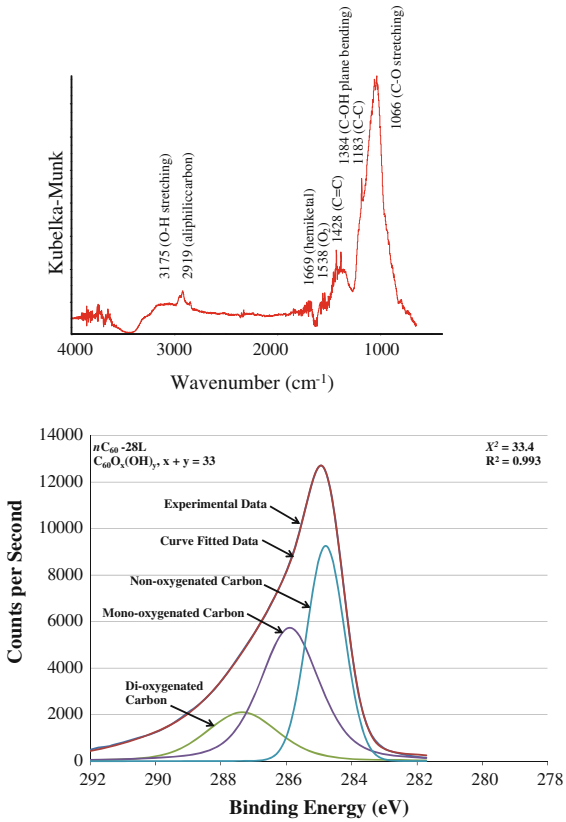

Fig. 4 FTIR (*top*) and XPS (*bottom*) spectra for *aqu-n*C_{60} stirred for 28 days exposed to light

were hemiketal (Chiang et al. 1993; Xing et al. 2004; An and Jin 2011), with peaks around 1,392, 1,426, and 1,658 cm^{-1}.

XPS spectra (Fig. 4 and Supplementary Information, Figs. SI-19, SI-20, SI-21) were normalized to adventitious carbon at 283.60 eV (Swift 1982). Ratios of oxygenated groups, as estimated from the area under the deconvoluted peaks, resulted in assigning 27–39 of the 60 carbon binding sites to non-oxygenated carbons at 284.60 eV (Palchan et al. 1989), 10–27 carbon binding sites to mono-oxygenated carbon at 286.45 eV (Beamson and Briggs 1992), and 6–11 carbon binding sites to di-oxygenated carbon from 288.50 (Jones et al. 1990) to 288.90 eV (Beamson and Briggs 1992); tri-oxygenated carbon at 289.50 eV (Gelius et al. 1970) was attributed to non-associated sodium carbonate precipitants. Based on the XPS spectra and applying the generic formula, $C_{60}O_x(OH)_y$, $x + y = 21–33$ oxygenated carbons and the number of surface groups increased with stirring duration and exposure to light (Supplementary Information, Table SI-S2), which is consistent with previous findings (Fortner et al. 2007). At t_7, dark-stirred suspensions were comprised of nearly equal mono-oxygenated and di-oxygenated carbons with 10 and 11 groups, respectively. The 7-L suspension had four additional oxygenated carbons but twice as many of the oxygenated carbons were mono-oxygenated compared to di-oxygenated. At t_{14}, the number of functionalized carbon in both dark-stirred and light-stirred suspensions increased as did the ratio of mono-oxygenated to di-oxygenated carbons. The occurrence of mono-oxygenated groups increased rapidly from t_0 to t_7 and then displayed more moderate growth at $t > 7$ days. Of particular interest was the transformation between t_7 and t_{14}, whereby the absolute number of di-oxygenated (hemiketal) groups declined 37 % for the dark-stirred suspensions and 25 % for the light-stirred suspensions. Between t_{14} and t_{28}, dark-stirred and light-stirred suspensions gained one and four additional mono-oxygenated carbon, respectively, while the number of di-oxygenated hemiketal groups remained unchanged.

The kinetics of surface group formation (Supplementary Information, Figure SI-S22) can be described through the relationship $g_i = a\ln(t) + b$, where g = number of surface groups of type i, t = stirring time, and parameters a and b (Supplementary Information, Table SI-S3) with R^2 of 0.9808 (dark-stirred) and 0.991 (light-stirred) for the combined total number of surface groups and 0.7136 (dark-stirred) and 0.8357 (light-stirred) for the di-oxygenated carbons. Dark-stirred suspensions appeared to have completed derivatization near t_{14}, with only one mono-oxygenated group being added during the final two weeks of stirring. The transformation of light-stirred suspensions did not appear to be complete during the 28-day synthesis period, as the number of mono-oxygenated groups continued to increase, suggesting future investigation examine derivatization exhaustion.

Derivatized fullerene chemical composition analysis is a developing science. Despite publications on surface groups associated with fullerene (Guirado-López and Rincón 2006; Satoh and Takayanagi 2006; Chao et al. 2011; Murdianti et al. 2012; Pycke et al. 2012; Jung et al. 2013), determination of definitive chemical composition within a limited surface group tolerance continues to be uncertain. Researchers have used a variety of characterization techniques without definitively quantifying fullerene surface derivatization

Table 1 Intramolecular vibrational modes for *aqu*-nC_{60}

Experimental data (cm^{-1})						Assigned vibrational characteristic
7D	7L	14D	14L	28D	28L	
803[a]	805[a]	850[b]			880[c]	C–H out-of-plane bending
940[d]	945[d]	979[d]	943[d]			C–O–C epoxide
1,066[e]	1,062[e]	1,063[e]	1,001	1,034[f]	1,050[g]	C–O
1,183[h]	1,185[h]	1,129[i]	1,129[i]	1,183[h]	1,183[h]	C–C, C–OH
1,384[j]	1,384[j]	1,384[j]	1,384[j]	1,384[j]	1,383[j]	Hemiketal, C–OH, or C–H symmetrical bending
1,428[k]	1,429[k]	1,453[l]	1,460[m]	1,431[k]	1,428[k]	Hemiketal, C–O, C–OH, or C–C
1,538[n]				1,577		C–O, CO_2, or C–C
1,669[p]	1,670[p]	1,679[q]	1,656[r]	1,679[q]	1,656[r]	Hemiketal, O–H covalent bond
2,364 [s]	2,364[s]	2,364[s]	2,364[s]	2,364[s]	2,364[s]	CO_2
2,919[t]	2,963[t]	2,920[t]	2,921[t]	2,920[t]	2,973[t]	CH_2 asymmetrical stretching
3,175[u]	3,172[u]					O–H stretching
3,627[v]		3,466[v]	3,431[v]	3,443[v]	3,317[v]	O–H stretching

[a] THF-nC_{60} (Lee et al. 2010); O–H out-of-plane bending in carbon nanotubes (Baudot et al. 2010)

[b] $C_{60}(OH)_n$ (Bogdanovic et al. 2004); C–O bond in $C_{60}(OH)_n$ (Isakovic et al. 2006)

[c] $C_{60}(OH)_n$ (Krishna et al. 2008)

[d] C–O epoxide (Tianbao et al. 1999); THF-nC_{60} (Lee et al. 2010)

[e] O–H in $C_{60}(OH)_n$ (Alves et al. 2006); C–O stretching in $C_{60}(OH)_n$ (Krishna et al. 2008); C–O in son-nC_{60} without solvent, and $C_{60}(OH)_n$ (Hwang and Li 2010); C–OH in-plane bending or O=C–O– in irradiated C_{60} (Hou and Jafvert 2009b)

[f] $C_{60}(OH)_n$ (Bogdanovic et al. 2004); C–O bond in $C_{60}(OH)_n$ (Semenov et al. 2011)

[g] C–OH stretching in C_{60} ozopolymer (Cataldo and Heymann 2006); C–O bond in $C_{60}(OH)_n$ (Husebo et al. 2004)

[h] C_{60} (Haufler et al. 1990; Bethune et al. 1991); $C_{60}O$ (Creegan et al. 1992); precipitate from THF-nC_{60} (Wei et al. 1997); C–O stretching in C_{60} ozopolymer (Cataldo and Heymann 2006); C_{60}, THF-nC_{60}, and $C_{60}(OH)_n$ (Isakovic et al. 2006; Harhaji et al. 2006); THF-nC_{60} (Fortner et al. 2007); C–C bond in son-nC_{60} no solvent (Labille et al. 2009); C_{60} (Hou and Jafvert 2009b); C_{60} in toluene (Bae et al. 2011); son-nC_{60} with toluene (Wang et al. 2012; An and Jin 2011)

[i] THF-nC_{60} (Lee et al. 2010); O–H out-of-plane bending in carbon nanotubes (Baudot et al. 2010)

[j] C–OH in-plane bending in C_{60} ozopolymer (Cataldo and Heymann 2006); O–H bending in $C_{60}(OH)_n$ (Zhang et al. 2003); water molecules in C_{60} in toluene (Bae et al. 2011); son-nC_{60} with toluene (Wang et al. 2012; An and Jin 2011)

[k] C_{60} (Hou and Jafvert 2009b; Haufler et al. 1990; Bethune et al. 1991); $C_{60}O$ (Creegan et al. 1992); precipitate from THF-nC_{60} (Wei et al. 1997); C_{60} and O–H bond in $C_{60}(OH)_n$ (Alves et al. 2006); THF-nC_{60} (Fortner et al. 2007); C–C in son-nC_{60} without solvent (Hwang and Li 2010); hemiketal in son-nC_{60} with toluene (An and Jin 2011); C_{60} in toluene (Bae et al. 2011); son-nC_{60} with toluene (Wang et al. 2012)

[l] C_{60} (Semenov et al. 2011; Bethune et al. 1991); C–OH bending in $C_{60}(OH)_n$ (Krishna et al. 2008); -O–H bending in $C_{60}(OH)_n$ (Chao et al. 2011)

[m] C_{60} (Bethune et al. 1991); C–H bending in C_{60} (Kamaras et al. 1993); C–H asymmetrical bending in C_{60} precipitated from C_{60} hydrosol (Andrievsky et al. 2002); C–C or C–H scissoring in $C_{60}(OH)_n$ (Hotze et al. 2008); son-nC_{60} with toluene (Wang et al. 2012)

[n] C_{60} (Bethune et al. 1991); clathrated CO_2 in C_{60} (Kamaras et al. 1993); C–O bond in C_{60} (Hou and Jafvert 2009b)

[o] Amorphous carbon structure in C_{60} (Sreseli et al. 2005)

[p] Hemiketal in $C_{60}(OH)_n$ (Krishna et al. 2008; Xing et al. 2004)

[q] O–H covalent bond in THF-nC_{60} (Isakovic et al. 2006)

[r] Hemiketal in $C_{60}(OH)_n$ (Xing et al. 2004)

[s] C–O in C_{60} (Hou and Jafvert 2009b)

[t] C–H asymmetrical bending in C_{60} precipitated from C_{60} hydrosol (Andrievsky et al. 2002); C–H asymmetrical stretching in THF-nC_{60} (Fang et al. 2007); THF-nC_{60} (Lee et al. 2007); C–H stretching in $C_{60}(OH)_n$ (Vileno et al. 2010); C–H bond in C_{60} (Bae et al. 2011)

[u] O–H bond in $C_{60}(OH)_n$ (Krishna et al. 2008); O–H stretching in $C_{60}(OH)_n$ (An and Jin 2011)

[v] O–H stretching in son-nC_{60} without solvent (Labille et al. 2009); $C_{60}(OH)_n$ (Bodganovic et al. 2004; Zhang et al. 2003; Chiang et al. 1993; Mirkov et al. 2004; Icevic et al. 2011); O–H stretching in $C_{60}(OH)_n$ (Chao et al. 2011; Krishna et al. 2008, p. 65; An and Jin 2011; Xing et al. 2004; Li et al. 1993; Schreiner et al. 2009)

moieties or determining formation pathway. FTIR spectroscopy has been used to identify surface groups found in association with fullerene species (Ibrahim and El-Haes 2005; Troshin et al. 2006; Chao et al. 2011; Wang et al. 2012), but has not been used reliably to quantify these groups. XPS studies (Fortner et al. 2007; Lee et al. 2009; Hwang and Li 2010; Qu et al. 2012) have been used to quantify carbon oxygenation states (e.g., non-oxygenated, mono-oxygenated, etc.) but overlapping peaks prohibit differentiation of specific surface groups. Due to scarcely detectable differences in bond energies of the oxygenation states (i.e., $\Delta E < 1.5$ eV between non-oxygenated and mono-oxygenated carbon bond energies), computer algorithms must be employed to deconvolute XPS spectra, providing an estimate of quantification, obfuscating precise compositions of surface groups, thus complicating assessment of biological effects. Despite the efforts conducted to date, the most candid representation of the chemical composition of *aqu-n*C_{60} and other derivatized fullerene species is semi-quantitative.

Formation of derivatized *aqu-n*C_{60}

The introduction of C_{60} to water disrupted entropic equilibrium in the solvent, isolating the non-polar material (and the associated energy increase) within the aqueous medium, thus lowering system entropy to a localized minimum. The presence of a hydrated layer around clusters of underivatized fullerene suggests that reorganization of water molecules contributed to fullerene dispersability. In addition, fullerene molecules facilitated colloid formation by reducing the contribution to interfacial tension and entropy increase through the formation of clusters, minimizing surface area and, consequently, the interfacial surface, which further reduced the energy differential. The method used to quantify the carbon oxygenation states assumed that the only influence on spectra was derivatized *aqu-n*C_{60} with surface functional groups. A potential shortfall of this approach was that not all of the molecules scanned by the XPS system were derivatized, based on a scanning depth of 5.0 nm (Carlson 1978); the diameters of underivatized fullerene and *aqu-n*C_{60} were 0.7 and 1.3 nm, respectively, as determined through geometrical constructs. Data indicated that between 45 and 65 % of the carbon atoms scanned were oxygenated, suggesting the aggregate surface was comprised of several concentric layers of derivatized fullerene surrounding underivatized molecules. Such an agglomerate configuration indicates that the degree of derivatization of the layers followed a gradient, with more-derivatized and hydrophilic molecules closer to the liquid–solid interface and less-derivatized molecules closer to the agglomerate center.

Aravand and Semsarzadeh (2008) showed that stirring velocity impacted the size of epoxy emulsions formed at the submicron-scale, suggesting a similar relationship with other materials such as fullerene; yet, despite consistency in aspect ratios over time, shaping of the clusters did occur, as was observed in the TEM images (Fig. 3). Clusters shown at t_{14} appeared with greater irregularity of form than those at t_f and smaller primary groups were visibly adhered to the bulk solid at t_{14}. Aggregates viewed at t_{28} did not decrease significantly in size but rather appeared with smoother edges (Fig. 3), suggesting that primary groups at $t < 28$ days were attached to agglomerates with forces that were unable to withstand shear caused by stirring, and while mean agglomerate size did not change significantly over time, the distribution of sizes narrowed.

Several observations from the *aqu-n*C_{60} chemical composition analysis provided insight to the pathways and mechanisms potentially involved in the dispersion of fullerene. XPS data showed the number of surface groups increased when stirring occurred in light, indicating photo-active derivatization. Dark-stirred suspensions had more hemiketal groups but fewer mono-oxygenated groups than light-stirred suspensions prepared over the same duration, which suggests that exposure to light caused surface groups to favor the mono-oxygenated carbon state. The number of total and mono-oxygenated surface groups increased over time, while the number of di-oxygenated hemiketal groups decreased over time, demonstrating that the input of mechanical energy impacted number and type of surface groups. Further, it was determined through FTIR that epoxide groups decreased over time, from being measureable at t_7 and t_{14} to not being detected at t_f regardless of photocondition.

Protonation and hydration were thought to be the initial steps in *aqu-n*C_{60} agglomerate synthesis. Based on results from molecular dynamic simulation (Ajie et al. 1990), a highly dynamic system was proposed, whereby water molecules were organized loosely around C_{60} with the electronegative oxygen facing the

electrophilic, hydrophobic fullerene molecule and presenting the hydrogen end to the aqueous medium, which facilitated dispersion. Protonated species were reported to be less hydrophilic than the parent material (Ajie et al. 1990; McElvany and Callahan 1991), suggesting the propensity for agglomeration was elevated with hydrogen bound to the surface of the fullerene due to increased hydrophobic forces. Protonated fullerene was shown to be more effective in forming a hydrated layer with less fleeting interactions as water molecules formed hydrogen bonds with $C_{60}H_x$ (Haufler et al. 1990; Chiang et al. 1993; Kroto et al. 1994; Brant et al. 2005). Continued stirring may have promoted interaction at the agglomerate interface, facilitating derivatization with oxygenated surface groups.

Murdianti et al. (2012) indicated that the presence of ozone or previously epoxylated fullerene was necessary for epoxylated fullerene formation, yet posed that no subsequent surface derivatization of *aqu-n*C_{60} occurs. Other studies have proposed the first derivatized state in *aqu-n*C_{60} transformation was attachment of two hydroxyl groups through reduction of the π-bonded carbons (at the intersection of hexagonal faces), resulting in 1,2-dihydroxylated [C_{60}]fullerene, or *vic*-diol fullerene (Chiang et al. 1993; Kong et al. 2009). Hydroxyl moieties on the surface of C_{60} exhibit high potential for steric interference, promoting transformation of the hydroxyl groups to a single epoxide moiety followed by conversion to an ether group through redistributing the electrons within the σ-bond of associated carbon atoms. After additional hydroxylation at one of the involved carbon sites, creation of a hemiketal structure is feasible (Chiang et al. 1993). Numerous researchers have documented the formation of isolated oxygen species on the carbon cage (Chiang et al. 1993; Tianbao et al. 1999; Xing et al. 2004), mainly under the presumption that these groups were transformed to or from ether, hemiketal, or epoxide groups. This pathway (Fig. 5) was determined to be reversible through this study, demonstrated by the instability of some species, specifically epoxide and hemiketal groups, which appeared with greater frequency at earlier sampling events.

Molecular transformation of the fullerene surface could be attributed to mechanical processes such as resonance transfer energy instigated by intermolecular collisions, chemical processes such as hydrolysis or from a pH-shift caused by the generation of carbonic acid in solution, or photochemical processes with ROS in the presence of light. As agglomerates collided, nominally sized primary fullerene groups may have been shorn, adding to the total number of agglomerates, which increased the probability of interaction in a positive feedback mechanism. Mechanical energy enabled derivatization but only until diameters were achieved with adhesive forces adequate to withstand mechanically induced shear forces. Given an adequate amount of time, fewer primary fullerene agglomerates were available for displacement, resulting in a decline of the interaction rate. This decrease in the rate derivatization was anticipated given that each fullerene molecule has a limited number of π-bonds, the number of π-bonds decreases with each attached surface group, and the stirring rate decreased over time due to the constraint of maintaining a vortex of 50 % column height during synthesis.

The rate of derivatization decreased for both dark-stirred and light-stirred suspensions over the stirring period; surface derivatization appeared to stagnate in the dark-stirred suspensions at $t > 14$ days, but a notable derivatization rate (two surface groups weekly) was maintained in light-stirred suspensions until t_f. It is interesting to note that only mono-oxygenated groups were added during the final two weeks of stirring under both photoconditions, suggesting that conditions for di-oxygenated group formation and maintenance were only ideal in the first two weeks of stirring, perhaps as a result of a change in available DO. As photocondition was the primary difference in the experimental trials, exposing C_{60} to light was determined to prolong the active derivatization period and to favor mono-oxygenated surface groups over di-oxygenated moieties (Fig. 5).

Equilibrium chemistry suggests that a suspension with higher pH would be more favorable to the formation of hydroxylated groups, either of a mono-oxygenated *vic*-diol or a di-oxygenated hemiketal configuration. It was observed that the quantity of di-oxygenated hemiketal groups decreased in both dark-stirred and light-stirred suspensions between t_7 and t_{14}, and then remained unchanged for the duration of the test, indicating late-stage surface group enhancement occurred only through the addition of or conversion to mono-oxygenated hydroxyl groups. There was no significant difference in the rate of pH change between t_{14} and t_{28}, supporting the premise that pH did not affect surface group quantities. Epoxide moieties were

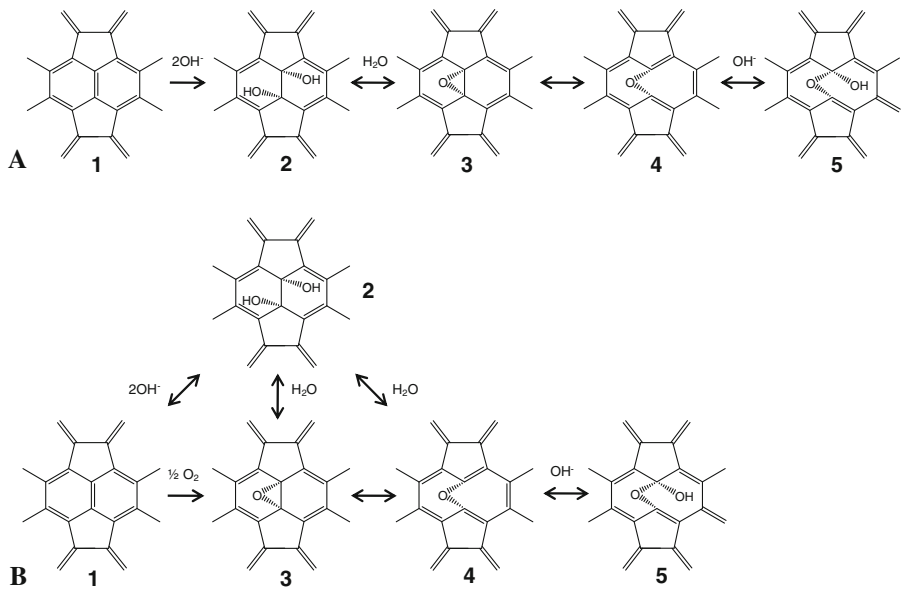

Fig. 5 Proposed primary (**a**) and alternate (**b**) pathway for *aqu-n*C_{60} surface group formation. The hydrogenated state of fullerene ($C_{60}H_x$) was omitted for clarity. *1* Underivatized fullerene; *2* hydroxylated fullerene; *3* epoxy-fullerene; *4* ether surface group; and, *5* hemiketal surface group

present at t_7 and t_{14}, which were marked by stagnant (light-stirred: Week 1), declining (dark-stirred: Week 1), and increasing (dark-stirred and light-stirred: Week 2) changes in pH. The pH range for all suspensions at $t \leq 14$ days, when epoxide groups were noted, was 4.42 to 5.96, indicating that epoxy-fullerene was only formable in a more-acidic environment. Epoxy–fullerene appeared to be the least stable oxygenated condition, perhaps a result of carbon–carbon–oxygen bond angles of 61.5 degrees, which lends to heightened physical strain energy of 25 kcal/mol (Wade 1998) and a tendency to exist as an unstable intermediate species. Disappearance of epoxide groups occurred between t_{14} and t_{28}, when the pH increased at the same rate as between t_7 and t_{14}, suggesting a critical pH at which epoxides disappeared rather than a linear relationship between acidity and surface groups. The range of critical pH was proposed between 5.9 and 6.1, as the former represents the light-stirred suspension at t_{14}, the highest recorded pH with the presence of epoxide, while the latter represents the dark-stirred suspension at t_{28}, the lowest recorded pH without the presence of epoxide.

By-products of *aqu-n*C_{60} preparation

FTIR spectra for residues, or by-products, from the synthesis process (Supplementary Information, Figs. SI-S23, SI-S24) indicated staunch consistency with underivatized C_{60} with the exception of a prominent peak at 3,434 cm^{-1}, which is typical of the hydroxyl bond of entrained water molecules, and several minor peaks, which can be attributed also to the material having been previously wetted or the formation of a hydrated layer. XPS spectrum for WASTE-*n*C_{60}-14L indicated that the material contained a single surface group, a mono-oxygenated moiety [$C_{60}H_z(OH)_n$ or $C_{60}H_zO_n$], while WASTE-*n*C_{60}-28L indicated the presence of nine mono-oxygenated groups, suggesting a chemical composition of $C_{60}H_zO_x(OH)_y$, $x + y = 9$; these surface groups could be any combination of hydroxyl, ether groups, or oxygen ions.

Conclusion

This study investigated the effect of light and synthesis duration on dispersion of C_{60} in water and the presence of functional groups on C_{60} agglomeration, proposing transformation kinetics of derivatized fullerene species. While UV/Vis spectra was unable to establish a statistically reliable predictor of surface derivatization, applications from this investigation include development of a predictor model for *aqu-n*C_{60} agglomerate concentrations, indicating increased derivatization as a function of

time as well as with light. It should be noted that agglomerate sizes did not differ significantly over the 28-day stirring period regardless of photocondition. The kinetics of surface group formation have been described through logarithmic relationships. Earlier-phase stirring ($t \leq 14$ days) products were shown to contain epoxide surface groups, while late-stage surface group enhancement was associated with the addition of mono-oxygenated hydroxyl groups only. In addition, exposure to light was determined to prolong the active derivatization period in favor of mono-oxygenated moieties. The disappearance of epoxide groups in late-phase stirring suggested a critical pH at which epoxides disappeared rather than a linear relationship between pH and surface group type and/or number. This information is helpful in designing aqueous C_{60} clusters for studying biological interaction of C_{60} for toxicological evaluation with desired functionalized groups as well as understanding the mechanisms associated with the transformation of other derivatized fullerene species with a variety of functionalized groups, especially those containing oxygenated moieties, in natural and man-made environments.

Acknowledgments This work was supported by the National Science Foundation (NSF Grant EEC-94-02989), the Particle Engineering Research Center at the University of Florida, and Ben Koopman, Ph.D.

References

Ajie H, Alvarez MM, Anz SJ, Beck RD, Diederich F, Fostiropoulos K, Huffman DR, Kratschmer W, Rubin Y, Schriver KE, Sensharma D, Whetten RL (1990) Characterization of the soluble all-carbon molecules C_{60} and C_{70}. J Phys Chem 94:8630–8633

Alves GC, Ladeira LO, Righi A, Krambrock K, Calado HD, Gill RP, Pinheiro MVB (2006) Synthesis of $C_{60}(OH)_{18\text{-}20}$ in aqueous alkaline solution under O_2-atmosphere. J Braz Chem Soc 17(6):1186–1190

An H, Jin B (2011) DNA exposure to buckministerfullerene (C_{60})—toward DNA stability reactivity and replication. Environ Sci Technol 45:6608–6616

Andrievsky GV, Klochkov VK, Bordyuh AB, Dovbeshko GI (2002) Comparative analysis of two aqueous-colloidal solutions of C_{60} fullerene with help of FTIR and UV–Vis spectroscopy. Chem Phys Lett 364:8–17

Aravand MA, Semsarzadeh MA (2008) Particle formation by emulsion inversion method: effect of the stirring speed on inversion and formation of spherical particles. Macromol Symp 274:141–147

Arbogast JW, Darmanyan AP, Foote CS, Rubin Y, Diederich FN, Alvarez MM, Anz SJ, Whetten RL (1991) Photophysical properties of C_{60}. J Phys Chem 95:11–12

Baati T, Bourasset F, Gharbi N, Njim L, Abderrabba M, Kerkeni A, Szearc H, Moussa F (2012) The prolongation of the lifespan of rats by repeated oral administration of [60] fullerene. Biomater 33(19):4936–4946

Badireddy AR, Budarz JF, Chellam S, Wiesner MR (2012) Bacteriophage inactivation by UV-A illuminated fullerenes—role of nanoparticle-virus association and biological targets. Environ Sci Technol 46:5963–5970

Bae E, Kwak BK, Kim W, Kim Y, Choi K, Yi J (2011) Synthesis of mono-dispersed nano-scale fullerene (C_{60}) crystals. J Nanosci Nanotechnol 11:3516–3522

Baudot C, Tan CM, Kong JC (2010) FIT spectroscopy as a tool for nano-material characterization. Infrared Phys Technol 53(6):434–438

Beamson G, Briggs D (1992) High resolution XPS of organic polymers: the Scienta ESCA300 database. Wiley, New York

Bensasson RV, Bienvenue E, Dellinger M, Leach S, Seta P (1994) C_{60} in model biological systems—a visible-UV absorption study of solvent-dependent parameters and solute aggregation. J Phys Chem 98:3492–3500

Bethune DS, Meijer G, Tang WC, Rosen HJ, Golden WG, Seki H, Brown CA, de Vries MS (1991) Vibrational Raman and infrared spectra of chromatographically separated C_{60} and C_{70} fullerene clusters. Chem Phys Lett 179(1–2):181–186

Bethune D, Meijer G, Tang W, Rosen H, Golden W, Seki H, Brown C, de Vries M (1999) Vibrational Raman and infrared spectra of chromatographically separated C_{60} and C_{70} fullerene clusters. Chem Phys Lett 179(1–2):181–186

Bogdanovic G, Kojic V, Dordevic A, Canadanovic-Brunet J, Vojinovic-Miloradov M, Baltic VV (2004) Modulating activity of fullerol $C_{60}(OH)_{22}$ on doxorubicin-induced cytotoxicity. Toxicol Vitro 18:629–637

Bouchard D, Ma X, Isaacson C (2009) Colloidal properties of aqueous fullerenes: isoelectric points and aggregation kinetics of C_{60} and C_{60} derivatives. Environ Sci Technol 43:6597–6603

Brant J, Lecoanet H, Wiesner M (2005) Aggregation and deposition characteristics of fullerene nanoparticles in aqueous systems. J Nanoparticle Res 7:545–553

Brant JA, Labille J, Bottero J, Wiesner MR (2006) Characterizing the impact of preparation method on fullerene cluster structure and chemistry. Langmuir 22:3878–3885

Brunet L, Lyon D, Alvarez P, Wiesner M (2009) Comparative photoactivity and antibacterial properties of C60 fullerenes and titanium dioxide nanoparticles. Environ Sci Technol 43:4355–4360

Bucher J, Masten S, Moudgil B, Powers K, Roberts S, Walker N (2004) Developing experimental approaches for the evaluation of toxicological interactions of nanoscale materials. U.S. Department of Health and Human Services

Carlson TA (1978) X-ray photoelectron spectroscopy. Academic Press, Maryland Heights

Cataldo F, Heymann D (2006) A study of polymeric products formed by C_{60} and C_{70} ozonation. Polym Degrad Stab 70:237–243

Chao T, Song G, Hansmeier N, Westerhoff P, Herckes P, Halden RU (2011) Characterization and LC-MS–MS based quantification of hydroxylated fullerenes. Anal Chem 83(5):1777–1783

Chen KL, Elimelech M (2009) Relating colloidal stability of fullerene (C_{60}) nanoparticles to nanoparticle charge and

electrokinetic properties. Environ Sci Technol 43:7270–7276

Chiang LY, Upasani RB, Swirczewski JW, Soled S (1993) Evidence of hemiketals incorporated in the structure of fullerols derived from aqueous acid chemistry. J Am Chem Soc 115:563–5457

Creegan KM, Robbins JL, Robbins WK, Millar JM, Sherwood RD, Tindall PJ, Cox DM, Smith AB, McCauley JP, Jones DR, Gallagher RT (1992) Synthesis and characterization of $C_{60}O$ the first fullerene epoxide. J Am Chem Soc 114:1103–1105

Dai J, Wang C, Shang C, Graham N, Chen G (2012) Comparison of the cytotoxic responses of *Escherichia coli* (*E. coli*) AMC 198 to different fullerene suspensions (nC_{60}). Chemosphere 87:362–368

Dean RB, Dixon WJ (1951) Simplified statistics for small numbers of observations. Anal Chem 23(4):636–638

Deguchi S, Alargova RG, Tsujii K (2001) Stable dispersions of fullerenes, C_{60} and C_{70}, in water. Preparation and characterization. Langmuir 17:6013–6017

Dhawan A, Taurozzi JS, Pandey AK, Shan W, Miller SM, Hashsham SA, Tarabara VV (2006) Stable colloidal dispersions of C fullerenes in water: Evidence for genotoxicity. Environ Sci Technol 40:7394–7401

Fang J, Lyon DY, Wiesner MR, Dong J, Alvarez P (2007) Effect of a fullerene water suspension on bacterial phospholipids and membrane phase behavior. Environ Sci Technol 41(7):2636–2642

Fortner JD, Lyon DY, Sayes CM, Boyd AM, Falkner JC, Hotze EM, Alemany LB, Tao YJ, Guo W, Ausman KD, Colvin VL, Hughes JB (2005) C_{60} in water: nanocrystal formation and microbial response. Environ Sci Technol 39:4307–4316

Fortner JD, Kim D, Boyd AM, Falkner JC, Moran S, Colvin VL, Hughes JB, Kim J (2007) Reaction of water-stable C_{60} aggregates with ozone. Environ Sci Technol 41:7497–7502

Gao J, Wang Y, Folta KM, Krishna V, Bai W, Indeglia P, Georgieva A, Nakamura H, Koopman B, Moudgil B (2011) Polyhydroxy fullerenes (fullerols or fullerenols): beneficial growth and lifespan in diverse biological models. PLoS ONE 6(5):1e7

Gelius U, Heden PF, Hedman J, Lindberg BJ, Marine R, Nordberg R, Nordling C, Siegbahn K (1970) Molecular spectroscopy by means of ESCA. Phys Scr 2:70–80

Guirado-López RA, Rincón ME (2006) Structural and optical properties of highly hydroxylated fullerenes: stability of molecular domains on the C_{60} surface. J Chem Phys 125:1–10

Hancock DE, Indest KJ, Gust KA, Kennedy AJ (2012) Effects of C_{60} on the *Salmonella typhimurium* TA100 transcriptome expression: insights into C_{60}-mediated growth inhibition and mutagenicity. Environ Toxicol Chem 31:1438–1444

Harhaji L, Raicevic N, Romcevic N, Vailjevic-Radovic D, Dramicanin M, Trajkovic V (2006) Inactivation of nanocrystalline C_{60} cytotoxicity by γ-irradiation. Biomaterials 27:5049–5058

Haufler RE, Conceicao J, Chibante PF, Chai Y, Byrne NE, Flanagan S, Haley MM, O'Brien SC, Pan C, Xiao Z, Billups WE, Ciufolini MA, Hauge RH, Margrave JL, Wilson LJ, Curl RF, Smalley RE (1990) Efficient production of C_{60} and $C_{60}H_{36}$ and the solvated buckide ion. J Phys Chem 94:8634–8636

Henry T, Menn F, Fleming J, Wilgus J, Compton R, Sayler G (2007) Attributing effects of aqueous C_{60} nano-aggregates to tetrahydrofuran decomposition products in larval zebrafish by assessment of gene expression. Environ Health Perspect 115:1059–1065

Henry TB, Petersen EJ, Compton RN (2011) Aqueous fullerene aggregates (nC_{60}) generate minimal reactive oxygen species and are of low toxicity in fish: a revision of previous reports. Biotechnology 22:533–537

Heymann D (1996) Solubility of fullerenes C_{60} and C_{70} in water. Fullerene Sci Technol 4:543–544

Hotze EM, Labille J, Alvarez P, Wiesner MR (2008) Mechanisms of photochemistry and reactive oxygen production by fullerene suspensions in water. Environ Sci Technol 42:4175–4180

Hou W, Jafvert C (2009a) Photochemical transformation of aqueous C_{60} clusters in sunlight. Environ Sci Technol 43:362–367

Hou W, Jafvert C (2009b) Photochemistry of aqueous C_{60} clusters: evidence of $^1O_2$ formation and its role in mediating C_{60} phototransformation. Environ Sci Technol 43:5257–5262

Hou W, Moghadam BY, Westerhoff P', Posner JD (2011) Distribution of fullerene nanomaterials between water and model biological membranes. Langmuir 27:11899–11905

Husebo LO, Sitharaman B, Furukawa K, Kato T, Wilson LJ (2004) Fullerenols revisited as stable radical anions. J Am Chem Soc 126:12055–12064

Hwang YS, Li Q (2010) Characterizing photochemical transformation of aqueous nC_{60} under environmentally relevant conditions. Environ Sci Technol 44:3008–3013

Ibrahim M, El-Haes H (2005) Spectroscopic study of C_{60} and C_{80} and their epoxides. Chin J Phys 43(5):915–923

Icevic ID, Vukmirovic SN, Srdenovic BU, Suji JJ, Djordjevic AN, Injac RM, Vasovic VM (2011) Protective effects of orally applied fullerenol nanoparticles in rats after a single dose of doxorubicin. Hemijska Industrija 65:329–337

Isakovic A, Markovic Z, Todorovic-Markovic B, Nikolic N, Vranjes-Djuric S, Mirkovic M, Dramicanin M, Harhaji L, Raicevic N, Nikolic Z, Trajkovic V (2006) Distinct cytotoxic mechanisms of pristine versus hydroxylated fullerene. Toxicol Sci 91(1):173–183

Jones TS, Ashton MR, Richardson NV, Mack RG, Unertl WN (1990) The interaction of the polyimide precursors PMDA (1,2,4,5-benzenetetracarboxylic anhydride) and *m*-PDA (1,3-phenylenediamine) with Ni(110). J Vac Sci Technol A 8(3):2370–2375

Jung YK, Kim MJ, Kim Y, Kim JY (2013) Limitation of UV–Vis absorption analysis for determination of aqueous colloidal fullerene (nC_{60}) at high ionic strength. KSCE J Civ Eng 17(1):51–59

Kamaras K, Akselrod L, Roth S, Mittelbach A, Hiinle W, von Schnering HG (1993) The orientational phase transition in C_{60} films followed by infrared spectroscopy. Chem Phys Lett 214(3–4):338–344

Kong L, Zepp RG (2012) Production and consumption of reactive oxygen species by fullerenes. Environ Toxicol Chem 31(1):136–143

Kong L, Tedrow O, Chang YF, Zepp RG (2009) Light-initiated transformation of fullerenol in aqueous media. Environ Sci Technol 43:9155–9160

Kovochich M, Espinasse B, Auffan M, Hotze EM, Wessel L, Xia T, Nel AE, Wiesner MR (2009) Comparative toxicity of C_{60} aggregates toward mammalian cells: role of tetrahydrofuran (THF) decomposition. Environ Sci Technol 43:6379–6384

Krishna VB, Yanes D, Imaram W, Angerhofer A, Koopman B, Moudgil B (2008) Mechanisms of enhanced photocatalysis with polyhydroxy fullerenes. Appl Catal B 79:376–381

Kroto HW, Taylor R, Walton DRM (1994) The structure and reactivity of C_{60}. Pure Appl Chem 66(10–11):2091–2094

Labille J, Brant J, Villieras F, Pelletier M, Thill A, Masion A, Wiesner M, Rose J, Bottero JY (2006) Affinity of C_{60} fullerenes with water. Fuller Nanotub Carbon Nanostruct 14:307–314

Labille J, Masion Am, Ziarelli F, Rose J, Brant J, Villieras F, Pelletier M, Borschneck D, Wiesner MR, Bottero J (2009) Hydration and dispersion of C_{60} in aqueous systems: the nature of water-fullerene interactions. Langmuir 25(19):11232–11235

Lee J, Fortner JD, Hughes JB, Kim J (2007) Photochemical production of reactive oxygen species by C_{60} in the aqueous phase during UV irradiation. Environ Sci Technol 41(7):2529–2535

Lee J, Cho M, Fortner JD, Hughes JB, Kim J (2009) Transformation of aggregated C_{60} in the aqueous phase by UV irradiation. Environ Sci Technol 43(13):4878–4883

Lee J, Song W, Jang SS, Fortner JD, Alvarez PJJ, Cooper WJ, Kim J (2010) Stability of water-stable C_{60} clusters to OH radical oxidation and hydrated electron reduction. Environ Sci Technol 44:3786–3792

Li J, Takeuchi A, Ozawa M, Li X, Saigo K, Kitazawa K (1993) C_{60} fullerol formation catalysed by quaternary ammonium hydroxides. J Chem Soc Chem Commun 23:1784–1785

Lyon DY, Adams LK, Falkner JC, Alvarez PJJ (2006) Antibacterial activity of fullerene water suspensions: effects of preparation method and particle size. Environ Sci Technol 40:4360–4366

Lyon D, Brunet L, Hinkal G, Wiesner M, Alvarez P (2008) Antibacterial activity of fullerene water suspensions (nC_{60}) is not due to ROS-mediated damage. Nano Lett 8(5):1539–1543

Ma X, Bouchard D (2009) Formation of aqueous suspensions of fullerenes. Environ Sci Technol 43:330–336

Makarova TL (2001) Electrical and optical properties of pristine and polymerized fullerenes. Semiconductors 35(3):243–278. Translated from Fizika i Tekhnika Poluprovodnikov 35(3):257–293

Makarova EG, Gordon RY, Podolski IY (2012) Fullerene C_{60} prevents neurotoxicity induced by intrahippocampal microinjection of amyloid-β peptide. J Nanosci Nanotechnol 12(1):119–126

Markovic Z, Todorovic-Markovica B, Kleuta D, Nikolica N, Vranjes-Djurica S, Misirkicb M, Vucicevicb L, Janjetovicb K, Isakovic A, Harhajib L, Babic-Stojica B, Dramicanina M, Trajkovic V (2007) The mechanism of cell-damaging reactive oxygen generation by colloidal fullerenes. Biomaterials 28:5437–5448

McElvany SW, Callahan JH (1991) Chemical ionization of fullerenes. J Phys Chem 95:6186–6191

Mirkov SM, Djordjevic AN, Andric NL, Andric SA, Kostic TS, Bogdanovic GM, Vojinovic-Miloradov MB, Kovacevic RZ (2004) Nitric oxide-scavenging activity of PHF $C_{60}(OH)_{24}$. Nitric Oxide 11:201–207

Murayama H, Tomonoh S, Alford JM, Karpuk ME (2004) Fullerene production in tons and more: from science to industry. Fuller Nanotub Carbon Nanostruct 12(1–2):1–9

Murdianti BS, Damron JT, Hilburn ME, Maples RD, Koralege RSH, Kuriyavar SI, Ausman KD (2012) C_{60} oxide as a key component of aqueous C_{60} colloidal suspensions. Environ Sci Technol 46:7446–7453

Nardes AM, Ayzner AL, Hammond SR, Ferguson AJ, Schwartz BJ, Kopidakis N (2012) Photoinduced charge carrier generation and decay in sequentially deposited polymer/fullerene layers: bulk heterojunction vs. planar interface. J Phys Chem C 116:7293–7305

Oberdorster E (2004) Manufactured nanomaterials (C_{60}) induce oxidative stress in the brain of juvenile largemouth bass. Environ Health Perspect 112(10):1058–1062

Oberdorster E, Zhu S, Blickley T, McClellan-Green P, Haasch M (2006) Ecotoxicology of carbon-based engineered nanoparticles: effects of C_{60} on aquatic organisms. Carbon 44:1112–1120

Palchan I, Crespin M, Estrade-Szwarckopf H, Rousseau B (1989) Graphite fluorides: an XPS study of a new type of C–F bonding. Chem Phys Lett 157:321–327

Prylutska SV, Burlaka AP, Prylutskyy YI, Ritter U, Scharff P (2011) Pristine C_{60} fullerenes inhibit the rate of tumor growth metastasis. Exper Oncol 33(3):162–164

Pycke BFG, Chao T, Herckes P, Westerhoff P, Halden RU (2102) Beyond nC_{60}: strategies for identification of transformation products of fullerene oxidation in aquatic and biological samples. Anal Bioanal Chem 404:2583–2595

Qu X, Alvarez PJJ, Li Q (2012) Impact of sunlight and humic acid on the deposition kinetics of aqueous fullerene nanoparticles (nC_{60}). Environ Sci Technol 46:13455–13462

Ruoff RS, Tse DS, Malhotra R, Lorents DC (1993) Solubility of fullerene (C_{60}) in a variety of solvents. J Phys Chem 97(13):3379–3383

Satoh M, Takayanagi I (2006) Pharmacological studies on fullerene (C_{60}), a novel carbon allotrope, and its derivatives. J Pharm Sci 100:513–518

Schreiner KM, Filley TR, Blanchette RA, Bowen BB, Bolskar RD, Hockaday WC, Masiello CA, Raebiger JW (2009) White-rot basidiomycete-mediated decomposition of C_{60} fullerol. Environ Sci Technol 43:3162–3168

Semenov KN, Latenko DG, Charykov NA, Nikitin VA, Matuzenko MY, Keskinov VA, Postnov VN, Kopyrin AA (2011) Solubility and some properties of aqueous solutions of fullerenol-D and composition of crystal hydrates. Russ J Appl Chem 84(1):44–50

Snow SD, Lee J, Kim J (2012) Photochemical and photophysical properties of sequentially functionalized fullerenes in the aqueous phase. Environ Sci Technol 46:13227–13234

Sreseli OM, Zakharova IB, Vul SP, Makarova TL, Sharonova LV, Belyakov LV, Goryachev DN (2005) Interaction of fullerene with single-crystal silicon. Semiconductors 39(8):983–986. Translated from Fizika i Tekhnika Poluprovodnikov 39(8):1017–1020

Swift P (1982) Adventitious carbon: the panacea for energy referencing? Surf Interface Anal 4(2):47–51

Tervonen K, Waissl G, Petersen EJ, Akkanen J, Kukkonen VK (2010) Analysis of fullerene-C_{60} and kinetic measurements for its accumulation and depuration in *Daphnia magna*. Environ Toxicol Chem 29(5):1072–1078

Tianbao L, Xinhai L, Kexiong H, Hanying J, Jing L (1999) Synthesis and characterization of hydroxylated fullerene epoxide: an intermediate for forming fullerol. J Central South Univ Technol 6(1):35–36

Troshin PA, Peregudov AS, Lyubovskaya RM (2006) Reaction of [60]fullerene with $CF_3COOHal$ affords an unusual 1,3-dioxolano-[60]fullerene. Tetrahedron Lett 47:2969–2972

Vileno B, Jeney S, Siensiewicz A, Marcoux PR, Miller LM, Forro L (2010) Evidence of lipid peroxidation and protein phosphorylation in cells upon oxidative stress photo-generated by fullerols. Biophys Chem 152:164–169

Wade LG (1998) Organic chemistry, 3rd edn. Prentice Hall, Upper Saddle River

Wang C, Shang C, Ni M, Dai J, Jiang F (2012) (Photo)chlorination-induced physicochemical transformation of aqueous fullerene nC_{60}. Environ Sci Technol 46:9398–9405

Wei X, Wu M, Qi L, Xu Z (1997) Selective solution-phase generation and oxidation reaction of C_{60} and formation of an aqueous colloidal solution of C_{60}. J Chem Soc Perkin Trans 2:1389–1393

Xing G, Zhang J, Zhao Y, Tang J, Zhang B, Gao X, Yuan H, Qu L, Cao W, Chai Z, Ibrahim K, Su R (2004) Influences of structural properties on stability of fullerenols. J Phys Chem B 108:11473–11479

Yang Y, Nakada N, Nakajima R, Wang C, Tanaka H (2012) Toxicity of aqueous fullerene nC_{60} to activated sludge: nitrification inhibition and microtox test. J Nanomater. doi:10.1155/2012/512956

Zhang P, Pan H, Liu D, Guo Z, Zhang F, Zhu D (2003) Effective mechanochemical synthesis of [60]fullerols. Synth Comm 33(14):2469–2474

Zhou W, Xie S, Qian S, Wang G, Qian L (1996) Photothermal deflection spectra of solid C_{60}. J Condens Matter 8:5793–5800

Zhu X, Zhu L, Chen Y, Tian S (2009) Acute toxicities of six manufactured nanomaterials suspensions to *Daphnia magna*. J Nanopart Res 11:67–75